Hindawi
Advances in Civil Engineering
Volume 2023, Article ID 8037263, 20 pages
https://doi.org/10.1155/2023/8037263

Research Article

Settlement Prediction Based on the Relationship between the Empirical and Analytical Solutions of a Cylindrical Cavity under Undrained Conditions

Pieride Mabe Fogang [1,2] **Yang Liu** [1] **and Pengqiang Yu** [1]

[1] *School of Civil and Resource Engineering, University of Science and Technology Beijing, Beijing 100083, China*
[2] *Department of Earth Sciences, University of Yaoundé I, Yaoundé, P.O. Box 812, Cameroon*

Correspondence should be addressed to Yang Liu; yangliu@ustb.edu.cn

Received 14 March 2023; Revised 6 April 2023; Accepted 12 April 2023; Published 27 April 2023

Academic Editor: Sindy Seara-Paz

Settlements on the ground surface often relate to excavating an underground cavity in cities. Movement on the ground surface can create a void between the wall of the cylindrical cavity and the lining. Thus, this study proposes an approximate solution under undrained conditions, based on the relationship between the empirical and analytical methods for predicting ground settlement around a cylindrical cavity. Based on mathematical formulas, the results obtained by the geometrical representation are then associated with the experimental data. The study revealed that the settlement prediction is related either to ground surface loads or to the ground failure point. The expansion of the cylindrical cavity is solved as a linear elasticity problem using a system of first-order ordinary differential equations containing two components in the Cartesian coordinates. The stress distribution around the cylindrical cavity is evaluated based on a biaxial force. The proposed approaches show that the results (empirical and analytical) obtained are approximately similar. Hence, the relationship between the two methods can be best suited for predicting the settlement around a cylindrical cavity by evaluating both the maximum settlement and the maximum surface displacement.

1. Introduction

The increasing population in the developing countries has encouraged underground structure construction using advanced technologies to control ground motion and settlement. However, statistics have shown that the number of accidents in cavities is often determined by extreme loads and excavations on the ground surface (Huang and Zhang [1]). The difference of settlement between strata can cause ground cracking and severely threatens the safe construction and operation of underground engineering (Yan et al. [2]). Geotechnical engineers believe that the adverse effects on an ancient construction from underground excavations result from unavoidable changes in ground stress and motion (Klar and Marshall [3]; Klar et al. [4]; Avgerinos et al. [5]; Haji et al. [6]; Lu et al. [7]; Zhang et al. [8]). Based on in situ measurements, Wu et al. [9] proved that the settlement of the cylindrical cavity generating the subsidence is related to the compression of the upper soil layers. Nevertheless, prediction and mitigation of damages are essential factors in tunnel design.

The numerous attempts to develop predictive solutions for the ground behaviour are classified into the following three categories: the empirical method based on the Gaussian distribution curve (Peck [10]; Schmidt [11]; Celestino et al. [12]; Mo et al. [13]); numerical simulations relying on algorithms for model designs (Yan et al. [2]; Gioda and Swoboda [14]; Gao et al. [15]; Wang et al. [16]; Wu et al. [17]; Zhang et al. [18]; Möller and Vermeer [19]; Amorosi et al. [20]; Hasanpour [21]; Zheng et al. [22]; Zheng et al. [23]; Zhang et al. [24]; Zhang et al. [25]; Lü et al. [26]); and the analytical solution proposed to predict the ground behaviour (Sagaseta [27]; Verruijt and Booker [28]; Verruijt [29]; Park [30]; Wang et al. [31]; Pinto and Whittle [32]; Zhang et al. [25]; Mabe et al. [33]).

Moreover, a complex variable method has been proposed for the ground motion problem to avoid stresses imposed on the boundary conditions (Verruijt [29]). However, removing the additional weight of excavated ground generally causes soil to rebound, generating asymmetric stress redistribution (Verruijt and Booker [34]; Bobet [35]). Nonetheless, these ground movements should be conformal convergence and nonuniform deformation models, appropriate for estimating ground settlement in the near and far fields (Pinto and Whittle [32]). Most of these existing solutions were developed under the assumption that the cylindrical cavity would deform in an infinite medium (Yu and Rowe [36]; Mair [37]).

Li et al. [38] and Chen et al. [39] present a generic stress transport approach for the advanced solutions of the cylindrical cavity expansion under undrained and drained conditions. This solution is then modified by Zhang et al. [40] for undrained contraction problems. Thus, Chen and Abousleiman [41] propose an exact analytical solution in the undrained conditions using the rigorous definition of deviatoric stresses and a shear model that varies with the average soil pressure. Furthermore, the effects of rotational hardening, ignored by Chen et al. [42], have been recently included by Yang et al. [43] under drained loading conditions. Therefore, an exact general solution for the different ground models and a critical evaluation of various simplifying expressions were used by Vrakas [44] for the stress invariants around the cylindrical cavity.

Currently, many underground constructions use empirical and analytical approaches to predict settlements on the ground surface. These methods evaluate the resulting stresses from the settlement and then propose the solutions related to the progressive unloading of the cavity. Thus, based on the mathematical theorems, this study proposes the relationship between the empirical and analytical methods for predicting the ground deformation surrounding a cylindrical cavity. The significance and efficiency of the current solution obtained by the geometric representation are demonstrated by comparing it with the experimental data. Then, a comparative study of the two methods is performed to investigate the ground settlement under compression by the process of cavity expansion. Finally, a contribution of the obtained results is presented to show the applicability of the current solution in practical engineering.

2. Schematic Representation of the Cylindrical Cavity

Figure 1 represents the geometry of a cylindrical cavity in an infinite soil of initial radius r_0, in a biaxial plane of coordinates x and y, and of radial position r (radial distance from the axis of the cylindrical cavity) that is affected by the circumferential position of the soil $n\theta$ $(n \geq 1)$. For further explanation, Figure 1(a) shows an initial state of the soil at rest before the expansion of the cylindrical cavity defined by the following condition: horizontal stress equal to vertical stress $(\sigma_{x0} = \sigma_{y0})$. Furthermore, Figure 1(b) shows the expansion of a cylindrical cavity under hydrostatic compression, subjected to a horizontal effective pressure σ_{h0}, a vertical effective stress σ_{v0}, and a perpendicular effective stress σ_{z0}. During the expansion, two different regions are formed in Figure 1(b). The elastic region is at a considerable distance from the cavity, and the plastic region consists of two parts, namely, the softening zone and the residual zone. The conventional solution of the cylindrical cavity expansion is based on the idea that the in situ stress in a plane equals to $\sigma_{h0} = \sigma_{v0}$; thus, the stress distribution in the soil element is only affected by the radial position r (Hou et al. [45]). As the expansion pressure inside the cavity increases from the internal pressure p_0, the cavity expands from r_0 towards the plastic boundary. The internal pressure continues to increase, and the ground around the cavity gradually grows towards the radius of the plastic region r_p. At the deviation of the line between the elastic region and the plastic region is the elastoplastic region, which is the starting point of the radial displacement U_r. The cylindrical cavity is then subjected to a compression pressure between the ground surface pressure p_1 and the internal pressure p_0. Therefore, the initial stress components can be established by

$$\begin{aligned}
\sigma'_{r0} &= \sigma'_{h0}\cos^2\theta + \sigma'_{v0}\sin^2\theta,\\
\sigma'_{\theta 0} &= \sigma'_{h0}\sin^2\theta + \sigma'_{v0}\cos^2\theta,\\
\sigma'_{z0} &= \sigma'_{z0},\\
\tau_{r\theta 0} &= \left(\sigma'_{h0} - \sigma'_{v0}\right)\sin\theta\cos\theta.
\end{aligned} \tag{1}$$

The elastic limit diagram is circular with the radius of the cylindrical cavity (R). The expansion pressure of the internal cavity modifies the ground in the elastic region. Thus, the equilibrium equation in the polar coordinates can be defined as follows:

$$\frac{\partial\sigma_r}{\partial r} + \frac{\sigma_r - \sigma_\theta}{r} = 0, \tag{2}$$

where $\partial\sigma_r/\partial r$ is the derivative of the radial stress with respect to the radial position r, according to the Tresca criterion $(\sigma_\theta - \sigma_r = C_o)$, equation (2) can be restored as $\partial\sigma_r/\partial r - Co/r = 0$. Considering the shear affecting the horizontal cavity wall and the effect of the applied effective stress ($\sigma_{\text{eff}} = \sigma_T - U$; with U as the pore pressure) under the undrained condition, equation (2) can be redefined as follows:

$$\frac{\partial\sigma'_r}{\partial r} + \frac{\partial\left(\sigma_T - U\right)}{\partial r} + \frac{1}{r}\frac{\partial\tau'_{r\theta}}{\partial\theta} - \frac{Co}{r} = 0, \tag{3}$$

where $\partial(.)$ is the differential according to the Lagrangian description. When the soil is subjected to radial compression, the radial displacement U_r shown in Figure 1(b) can be expressed as $U_r = \left\{r^2 + \Delta_m^2 - r_p\left(2r_e - r_p\right)^2\right\}^{1/2} - r$, where $Dm = 2R$ is the diameter of the cylindrical cavity, R is the radius of the cylindrical cavity, r_p is the radius of the plastic region, and r_e is the radius of the elastic region. The soil elements around the cylindrical cavity first undergo elastic deformation and then plastic hardening with the

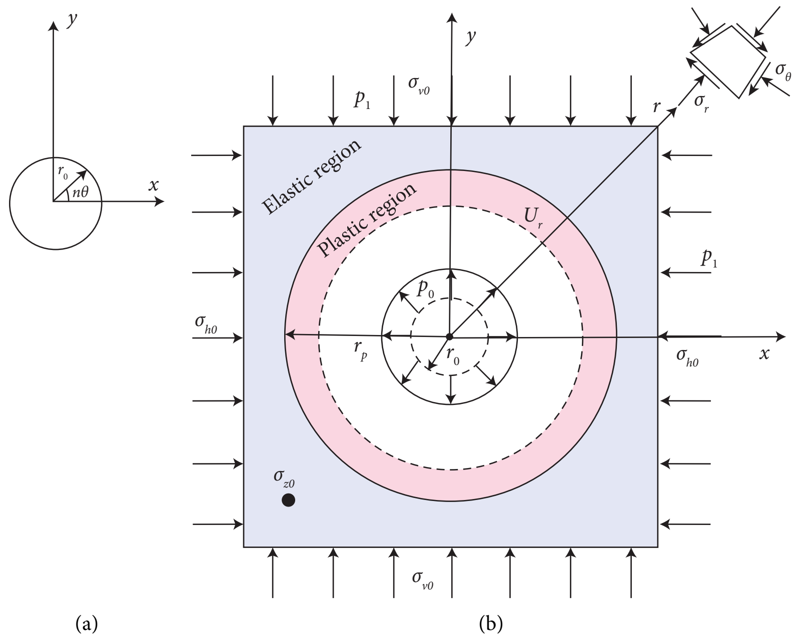

FIGURE 1: Geometric representation of the cylindrical cavity. (a) Initial ground state. (b) Cylindrical cavity expansion under hydrostatic compression.

degradation of the cavity wall (Zhai et al. [46]). Furthermore, the soil structure can be destroyed before reaching the boundary of the plastic region. In this vein, Zhuang et al. [47] explained that when the compression is positive, the initial stress at the cavity boundary condition can be given by $\sigma_r|r \longrightarrow r_0 = P_0$ and $\sigma_r|r \longrightarrow r_e = P_1$.

Since the differential system used in this study is Cartesian, two stress components are taken into account based on the theory of elasticity and plasticity. Thus, to derive the equation according to Mohr's circle, in the plane of stress, with a unit surface parallel to the direction of the $x - y$ plane (i.e., perpendicular to σ_{h0} and σ_{v0}), the effective stress and the effective shear stress can be obtained by the following expression:

$$\sigma_{\text{eff}} = \frac{1}{2}\left(\sigma_{x0} + \sigma_{y0}\right) + \frac{1}{2}\left(\sigma_{x0} - \sigma_{y0}\right)\cos 2\theta + \tau_{xy0}\sin 2\theta, \tag{4}$$

$$\tau_{\text{eff}} = -\frac{1}{2}\left(\sigma_{x0} - \sigma_{y0}\right)\sin 2\theta + \tau_{xy0}\cos 2\theta, \tag{5}$$

where σ_{x0} and σ_{y0} are stresses at the origin and τ_{xy0} is the initial shear stress. Next, a limited number of cases involving uniform vertical stress and inward shear stress are proposed by Gerrard [48] to solve the linear problem on a circular plane. Sivasithamparam and Castro [49] then adopt the condition that the direction of the known displacement vector at each point is independent of the stresses. The constitutive model can be obtained by using the boundary conditions. In the plane condition, when the cylindrical cavity expands, the displacement vector uses the shear stress to compensate for the "ovalization." The deformation field is then obtained from the elastic constitutive law.

When the tunnel is shallow, the stress deformation model is more influenced by the proximity to the stress-free ground surface (Pinto and Whittle [32]). Thus, for the ground deformation, the boundary conditions for the displacement of the cylindrical cavity wall are subdivided into the following three deformation models (as shown in Figure 2): (1). conformal convergence U_0 (with ground loss V_L), (2) vertical translation ΔU_y which is materialized by the downward movement, and (3) final form of displacement ΔU_f. Based on the deformation generated by the radius of the cylindrical cavity, the equation is as follows:

$$-U_0 = \Delta U_f - \Delta U_y. \tag{6}$$

According to Poulos [50], the influence factor of stress or displacement on a uniform load can be obtained by integrating the same element on a load point. As a theoretical tool for modelling engineering problems, the undrained cavity expansion solution is more urgent than the drained solution proposed by Zhai et al. [46]. An analysis of the settlement and maximum surface displacement around the cylindrical cavity is proposed, as well as the shear affecting the horizontal ground displacement.

3. Mathematical Evaluation of Displacements

This section proposes the mathematical theorems to predict the settlement around the cylindrical cavity. Airy stresses will be used as ground traction stresses, considering the loads on the ground surface. The method can be adapted to calculate displacements in directions other than the vertical direction and for loadings other than vertical direction (Poulos and Davis [51]).

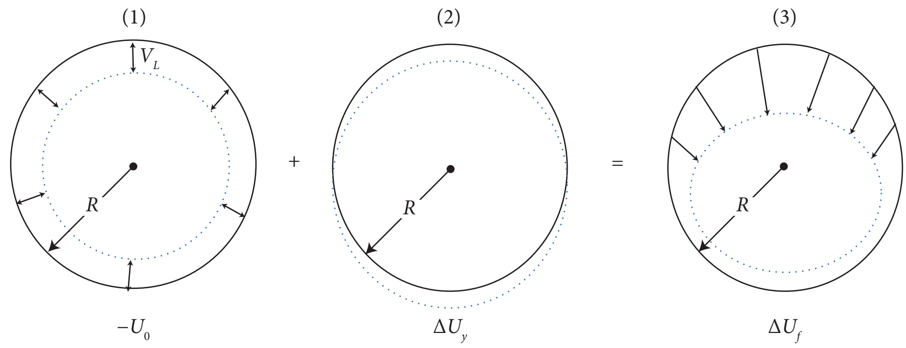

FIGURE 2: Different step of the ground deformation of a cylindrical cavity.

3.1. Empirical Evaluation of Ground Settlement. The behaviour of the deformed ground in the elastic region presented by Pinto et al. [52] is given by linear elasticity. Moreover, the cavity-induced horizontal ground displacements are analysed according to the ground settlement assumption (O'Reilly and New [53]). As suggested by Peck [10], the surface settlement trough shape is represented by the Gaussian distribution curve, which is defined as follows:

$$U_s = U_0 \max . \exp\left(-\frac{x_i^2}{2i^2}\right), \tag{7}$$

where U_s is the surface settlement, U_0 max is the maximum settlement from the ground surface towards the cylindrical cavity centerline, x_i is the standard deviation, and i is the inflection point of Gaussian curve, with $U_s/U_0 \max = 0.61$. The closed form solutions are evaluated by stress fields to limit the ground loss (Sagaseta [27]). The ground loss V_L can be calculated by using the relationship $V_L = 2\pi R u_\varepsilon$, where u_ε is the radial displacement at the wall of the cylindrical cavity. The inflection point involved the unloading of the cavity at different depths (Figure 3), which can be defined by $i = k(h - h_0)$. Mair et al. [54] proposed an empirical method to represent the subsurface settlement caused by the tunnel excavation using the following formula: $k = 0.5h - 0.325h_0/h - h_0$. Hence, the inflection point can be obtained by $i = 0.5h - 0.325h_0$. Using equation (7), the maximum settlement can be obtained as follows:

$$U_0 \max = 7.85u_\varepsilon . \frac{Rr^2}{k(h - h_0)}. \tag{8}$$

Next, using equation (6), the horizontal and vertical displacement (U_x, U_y) can be obtained by

$$U_x = -6.28u_\varepsilon \frac{h - 0.65h_0}{h - h_0} \frac{x(x + y)}{x^2 + y^2} R, \tag{9}$$

$$U_y = -3.14u_\varepsilon \frac{h + 0.65h_0}{h - h_0} \frac{y + h}{x^2 + y^2} R. \tag{10}$$

Then, the radial displacement U_r can be calculated by $(r^2 = x^2 + y^2)$

$$U_r = -\frac{6.28u_\varepsilon}{(h - h_0)} \left(\frac{R}{r}\right)^2 \left\{(x + y)(h - 0.65h_0)x^2 + (0.5h + 0.325h_0)(y + h)^2\right\}. \tag{11}$$

For $U_0 = U_y \max$ ($U_y \max$: maximum vertical displacement) and $h_0 = 0$, equations (9) and (10) become

$$U_x = -3.14u_\varepsilon R \left\{\frac{(x - 2)\left(x^2 - y^2\right) + x(\{5 - 2x\}y - h) + 2y}{\left(x^2 + y^2\right)^2}\right\}, \tag{12}$$

$$U_y = -3.15u_\varepsilon R \left(\frac{(x + 1)\left(x^2 - y^2\right) - y\left(2x^2 - x\right) - h(x - 2y)}{\left(x^2 + y^2\right)^2}\right). \tag{13}$$

Because ground settlement is established with $y = -h$ and $y = h$, respectively, equations (12) and (13) become

$$U_x = -3.14u_\varepsilon R\left\{\frac{(x-2)\left(x^2-(y+h)^2\right)+x(\{5-2x\}(y+h)-h)+2(y+h)}{\left(x^2+(y+h)^2\right)^2}\right\}, \tag{14}$$

$$U_y = -3.14u_\varepsilon R\left(\frac{(x+1)\left(x^2-(y+h)^2\right)-x(y+h)(2x-1)-h(x-2(y+h))}{\left(x^2+(y+h)^2\right)^2}\right), \tag{15}$$

$$U_x = -3.14u_\varepsilon R\left\{\frac{(x-2)\left(x^2-(y-h)^2\right)+x(5-2x)(y-2h)+2(y-h)}{\left(x^2+(y-h)^2\right)^2}\right\}, \tag{16}$$

$$U_y = -3.14u_\varepsilon R\left(\frac{(x+1)\left(x^2-(y-h)^2\right)-(y-h)(2x-1)x-h(x-2(y-h))}{\left(x^2+(y-h)^2\right)^2}\right). \tag{17}$$

When $y = -h$, for $x = 0$ (equation (14)), the horizontal displacement $U_x = 0$ and the maximum horizontal displacement $U_x \max = 0$. For $y = 0$, the maximum vertical displacement resulting from equation (15) becomes $U_y \max = -0.785u_\varepsilon (R/h)^2(1-3R/h)$. Next, for $y = \pm h$ and $x = 0$, the maximum horizontal displacement can be rewritten as $U_x \max = 0$. For $y = 0$ and $x = \pm h$, $U_y \max = -1.57u_\varepsilon$. Consequently, the vertical translation ΔU_y can be given by the following expression:

$$\Delta U_y = -6.28u_\varepsilon\left(\frac{R}{h}\right)^3\left(\frac{2(R/h)+1}{\left((R/h)^2+2\right)^2}\right). \tag{18}$$

For $R = \pm h$, equation (18) can be determined by $\Delta U_y \max = -2.09u_\varepsilon$. When $h^2 \gg R^2$, the shear stress can be given by $\tau_{xy} = -25.12u_\varepsilon RG.hx(((x^2-h^2)+1)/(x^2+h^2)^3)$. Using the Fourier transformation and respecting the yield of the spatial coordinates in equations (16) and (17), the components of the Airy stresses can be rewritten as follows:

$$\frac{\partial F}{\partial x} = 50.24xu_\varepsilon RG.h\left\{\frac{1-(2h-3y)x^2-(2h-3y)(y-h)^2}{\left(x^2+(y-h)^2\right)^3}\right\}, \tag{19}$$

$$\frac{\partial F}{\partial y} = 25.12u_\varepsilon RG.h\left\{\frac{\left(2x^2+(y-h)^2\right)x^2+\left(4\left(1+2hx^2\right)-(y-h)^3\right)(y-h)}{\left(x^2+(y-h)^2\right)^3}\right\}. \tag{20}$$

Therefore, the horizontal, vertical, and shear stress induced by the Airy stress can be established as follows, respectively:

$$\sigma_x = 50.24u_\varepsilon RG.h\left(\frac{\left(3yx^2+2\right)x^2+\left((y+8h)(y-h)^2-2x^2(y+11h)-10\right)(y-h)^2}{\left(x^2+(y-h)^2\right)^4}\right), \tag{21}$$

$$\sigma_y = -50.24u_\varepsilon RG.h\left\{\frac{\left\{\begin{array}{c}\left\{+2\left(h+y(y-h)^2\right)-(y+1)\right\}(y-h)^2-\ldots\\ -x^2\left(\begin{array}{c}(14h-11y)(y-h)^2-\ldots\\ +3(2h-y)+2\end{array}\right)-4(7h-2y)x^4\end{array}\right\}(y-h)^2+3x^4\left(1-\left(7x^2+2\right)(2h-y)\right)}{\left(x^2+(y-h)^2\right)^4}\right\}, \tag{22}$$

$$\tau_{xy} = 50.24u_\varepsilon RG.hx\left(\frac{6(y-h)+2(1-(y-h))x^4+9(y-h)^4+(y-h)\left(\begin{array}{c}2(y-h)(2(y-h)-5)+\ldots\\ +3(y+5h)\end{array}\right)x^2}{\left(x^2+(y-h)^2\right)^4}\right). \tag{23}$$

Therefore, the displacement induced by the surface settlement can be obtained as follows:

$$U_x = 12.56u_\varepsilon Rx\left\{\frac{(1-v)}{\left(x^2+(y-h)^2\right)}-4.\frac{1-(2h-3y)x^2-(2h-3y)(y-h)^2}{\left(x^2+(y-h)^2\right)^3}\right\}, \tag{24}$$

$$U_y = -12.56u_\varepsilon Rh\left\{\frac{(y-h)(1-v)}{\left(x^2+(y-h)^2\right)}+\frac{\left(2x^2+(y-h)^2\right)x^2+\left(4\left(1+2hx^2\right)-(y-h)^3\right)(y-h)}{\left(x^2+(y-h)^2\right)^3}\right\}. \tag{25}$$

Integrating equations (24) and (25), for $x = 0$, $U_x = 0$, and $U_x \max = 0$. For $y = 0$ and $x = \pm h$, $U_x \max = \pm 6.28u_\varepsilon(7-14v)(R/h)^2$. Therefore, equations (15), (17), and (25) can be rewritten as

$$\Delta U_y = -3.14u_\varepsilon\left(\frac{R}{h}\right)^2\left(\frac{4v(R/h)^4-36(R/h)^3+2(4v-17)(R/h)^2+4(R/h)+16}{\left((R/h)^2+2\right)^3}\right). \tag{26}$$

As the ground displacement around the cylindrical cavity is centered on the ground loss, the maximum vertical translation also coincides with the maximum settlement. Thus, the equilibrium shown in Figure 3 is satisfied. Consequently, equation (5) can be given by

$$U_s = \pm 1.57u_\varepsilon\left\{(1-4(2-v))^2-5\right\}\left(x_i^2-0.03\right).\exp\left\{-\frac{x_i^2}{0.061}\right\}\left(\frac{R}{h}\right)^2. \tag{27}$$

When the weight on the ground surface is large, the inner and outer pressure exerts a compressive stress, which changes the maximum ground settlement. The displacement-inducing stress fields are then considered as a hydrostatic compression state. Figure 3 shows the maximum ground settlement based on the ground behaviour at variable R/h, obtained from equation (5). For $R/h = 1$ (Figure 3(a)), $U_s \max(1) = -2.51$ m; $U_s \max(2) = -3.1$ m. For $R/h < 1$ (Figure 3(b)), U_s max

(1) = −2.3 m, and U_s max (2) = −2.7 m. The difference between these two curves results from the variation in U_s max. Therefore, the maximum depth of ground settlement is a function of the R/h ratio. Under static loading, the maximum settlement is high when the cylindrical cavity is shallow. Figure 4 summarises the displacement for $y = h$ and $y = -h$ (equations (14)–(17)), and the displacement induced by the shear stress (equations (24) and (25)) as a function of the ratio R/h and v. A significant influence of the Poisson ratio is again observed between $0.6 < R/h < 1$, with more significant corrections for lower Poisson ratio. Note that the results are similar to those obtained in Figure 4, using the vertical translation resulting from equation (26). Figure 5 shows the prediction of the horizontal and vertical displacement (U_x, U_y) of the soil around the cylindrical cavity, with the parameter $v = 0.25$, $u_\varepsilon = 1$ m, $R/h = 0.45$. Thus, taking into account the undrained condition adopted in this study (with the radius of the cylindrical cavity tending towards zero), the volume of soil loss remains constant if the displacement field is also constant.

3.2. Analysis of Ground Displacement. For the purpose of predicting ground deformation and displacement, an analytical solution based on the injection of compressive stresses is proposed. Gerrard [48] then proposes a complete set of solutions for stress, strains, and displacement at well-defined points in a two-dimensional system for the same variables. The estimation of these stresses is developed based on the linear elasticity problems. Using the ordinary differential equation (ODE), the radial displacement on the ground surface can be reformulated as $U_r = p_0/2G\{(1-2v)r + R^2/r\}$ (Pinto and Wittle [32]; Zhang et al. [25]; and Mabe et al. [33]). Hence, we can have

$$U_r = \frac{p_0}{2G}\left(r - \frac{R^2}{r}\right). \tag{28}$$

Or $u_\varepsilon = p_0 r/2G$ is the parameter of the conformal convergence. Hence, U_x and U_y components can be expressed as follows:

$$\begin{aligned} U_x &= u_\varepsilon x\left(\frac{x^2 + (y+h)^2 - R^2}{\left(x^2 + (y+h)^2\right)^2}\right), \\ U_y &= u_\varepsilon (y+h)\left(\frac{\left(x^2 + (y+h)^2\right) - R^2}{\left(x^2 + (y+h)^2\right)^2}\right), \end{aligned} \tag{29}$$

$$\begin{aligned} U_x &= u_\varepsilon x\left(\frac{x^2 + (y-h)^2 - R^2}{\left(x^2 + (y-h)^2\right)^2}\right), \\ U_y &= u_\varepsilon (y-h)\left(\frac{\left(x^2 + (y-h)^2\right) - R^2}{\left(x^2 + (y-h)^2\right)^2}\right). \end{aligned} \tag{30}$$

Using the Navier yield, the shear stress can be obtained as follows:

$$\tau_{xy} = 2u_\varepsilon G x(2y-h)\frac{2R^2 - \left(x^2 + (y-h)^2\right)}{\left(x^2 + (y-h)^2\right)^3}, \tag{31}$$

where τ_{xy} is the shear stress. For $y = 0$, the inverse Fourier transform $P_{(x,y)}$ can be defined by $P_{(x,y)} = 4u_\varepsilon RG\int_{-\infty}^{\infty}\{x/(x^2+h^2)\}e^{-i\omega x}d(x)$. Thus, the displacement induced by the inverse Fourier transformation and the shear stress can be calculated as follows:

$$U_x = \frac{1}{2}u_\varepsilon\left\{\frac{4R(1-v)x\left\{x^2 + R(y-h)^2\right\} + 3x^2R^2 - (y-h)^2\left(R^2 - (y-h)^2\right)}{\left(x^2 + (y-h)^2\right)^3}\right\}, \tag{32}$$

$$U_y = -\frac{1}{2}u_\varepsilon\left\{\frac{(y-h)(4R(1-v) - (y+h)) + x^2}{\left(x^2 + (y-h)^2\right)^2} + \frac{R^2\left\{(y-h)(3y+h) - x^2\right\}}{\left(x^2 + (y-h)^2\right)^3}\right\}. \tag{33}$$

Equation (28) can be rewritten as follows:

$$U_r = \frac{u_\varepsilon R}{2\left(x^2 + (y-h)^2\right)^3}\left\{\frac{x\left\{4xR(1-v)\left\{x^2 + R(y-h)^2\right\} - \cdots - (y-h)^2\left(R^2 - (y-h)^2\right)\right\} + R^2\left(3x^3 - (y+h)\left\{(y-h)(3y+h) - x^2\right\}\right)}{\left(x^2 + (y-h)^2\right)} + \cdots + (y+h)\left(x^2 + ((y+h) - 4R(1-v))(y-h)\right)\right\}. \tag{34}$$

Hence, for $y = 0$, equations (32) and (33) can be rewritten as follows:

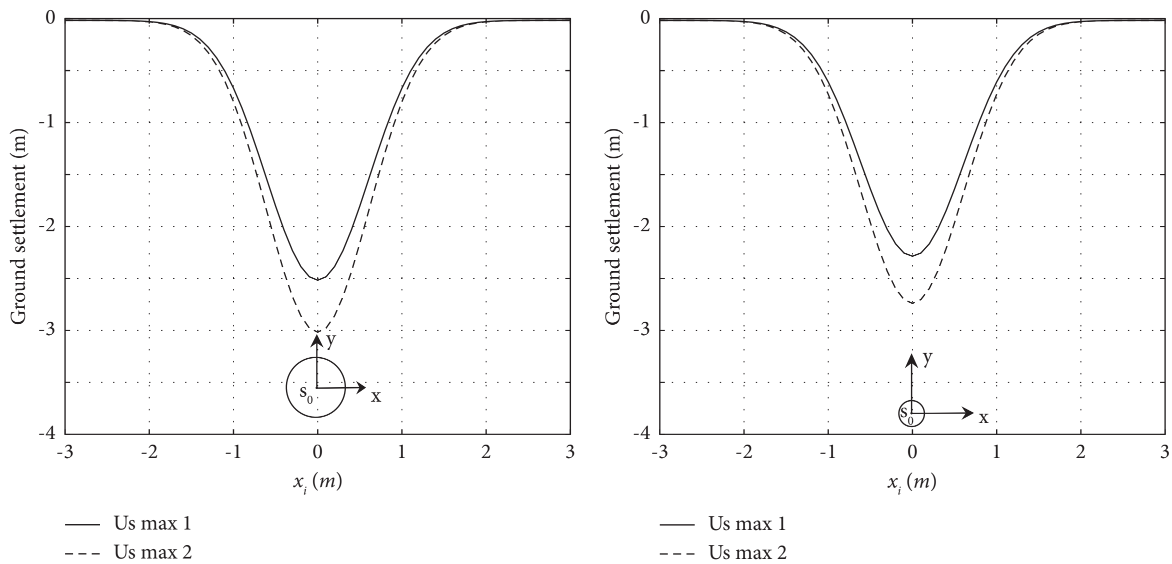

(a) (b)

FIGURE 3: Maximum settlement related to R/h variation. (a) $R/h = 1$. (b) $R/h < 1$.

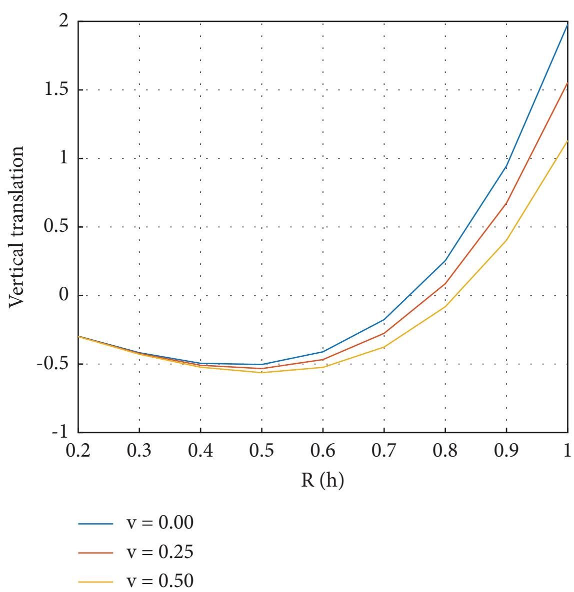

FIGURE 4: Vertical translation (empirical method).

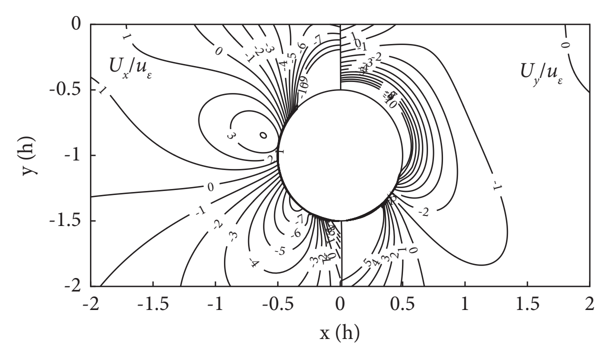

FIGURE 5: Stratigraphic contour based on the empirical method.

$$\tau_{xy} = u_\varepsilon G\left(\frac{3h\left(3x^3 - h^2\right)R^2 + h^3\left\{2h^2 - x^2\right\}}{\left(x^2 + h^2\right)^4} + \frac{x\left(11h^2 - x^2\right) + R^2(2x - 1) + 4x(2 + 5h)(1 - v)R}{\left(x^2 + h^2\right)^3}\right). \tag{35}$$

Hence, the maximum shear stress becomes $\tau_{xy}\max = -2u_\varepsilon G\left\{(R/h)^2 - 1\right\}$. Figure 6 shows a stratigraphic soil profile resulting from equations (29), (30), (32), and (33). Figures 6(a) and 6(b) show a horizontal and vertical displacement profile drawn on the transverse planes U_x/u_ε and U_y/u_ε. The contour lines are symmetrical and show transverse motion on the centreline of the cylindrical cavity for the value $x/h = 0$. The lines, all converge towards the centreline of the cavity. This is due to the decrease in the internal ground pressure. Using equation (32), for $y = 0$,

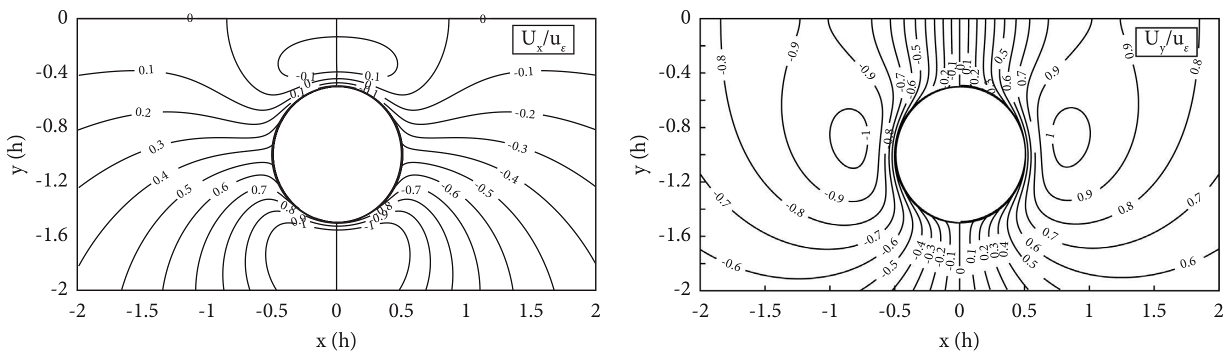

(a) (b)

Figure 6: Stratigraphic profile of a ground section around the cylindrical cavity. (a) Horizontal displacement. (b) Vertical displacement.

$U_y = 0$, and $U_y \max = 0$. Next, integrating equation (33), we can have

$$U_y = -u_\varepsilon \frac{1}{2}\left(\frac{R}{h}\right)\left\{\frac{\left(1+(x/h)^2\right)\left\{-4(1-\nu)(R/h)^2 + \left(1+(x/h)^2\right)\right\} + (R/h)^2\left\{1-(x/h)^2\right\}}{\left(1+(x/h)^2\right)^3}\right\}. \quad (36)$$

The maximum vertical displacement can be obtained by $(x = \pm h)$ $U_y \max = \pm 0.25 u_\varepsilon (1 - 2(1-\nu))$. The horizontal and vertical ground motions proposed numerically as follows: for $\Delta U_x = 0$, $\Delta U_x \max = 0$. Adding the equations (29), (30), and (33), the vertical translation can be obtained by the following formulas:

$$\Delta U_y = u_\varepsilon \left(\frac{R}{h}\right)^2 \left(\frac{(R/h)^2(2.5-2\nu) - 1.5}{\left((R/h)^2+2\right)^2}\right). \quad (37)$$

Figure 7 shows a vertical translation of the cross-section resulting from equation (33). For the variable Poisson ratio, all the curves converge to $R/h = 1$. The maximum settlement is represented by the following values: $\nu = 0$, $U_x \max = -0.04$ m; $\nu = 0.25$, $U_x \max = -0.05$ m; and $\nu = 0.50$, $U_x \max = -0.06$ m with $R/h = 0.6$. When $0.2 < R/h < 1$, the curves move downwards towards $R/h = 0.5$, while the interval $0.6 < R/h < 1$, the curves move upwards. When the load around the cylindrical cavity is low during ground compression, the wall of the cylindrical cavity can exert a "buoyancy" effect. According to Poulos and Davis [51], the method can be adapted to calculate displacements in directions other than the vertical direction for variable loads. Thus, the stresses will be equilibrated by applying a large force around the cavity.

4. Validation of Results

4.1. Ground Settlement. The data used to model the empirical part are represented by three tunnel models, one in London and two laboratory tests. The input parameters of the software are presented in Table 1. The tunnel radius and tunnel depth evaluation are represented by the ratio R/h with values of 0.12 (Ieronymaki et al. [55, 56]), $R/h = 0.31$ (Hu et al. [57]), and $R/h = 1$ (Wang et al. [58]), respectively. Under undrained conditions, the ground loss can also be evaluated as $V_L = 1 - (1 - (U_s \max / 2R))^2$. Therefore, for U_x max, the ground losses V_L and u_ε can be established as shown in Table 1.

4.1.1. Effect of U_x max. Figure 8 shows the maximum ground settlement obtained from the empirical formulas. The input parameters are U_x max, U_s, x_i, i, and V_L. Since the ground surface is planar, the maximum settlements obtained are symmetrical to the centre line at the value $x_i = 0$ m. The variables of U_x max shown in Figure 8(a) are −1.061 m, −1.12 m, −1.422 m, −1.5 m, −1.86 m, and −1.95 m. Then, U_x max for Figure 8(b) is given by −1.08 m, −1.437 m, −1.705 m, and −1.86 m. Finally, the U_x max for Figure 8(c) is given by −1.275 m, −1.44 m, −1.6 m, −1.63 m, −1.705 m, and −1.9 m. Using empirical analysis, $U_0 = -0.06$ m (Table 1 and Case 1), $U_0 = -0.06$ m (Table 1 and Case 2) and $U_0 = -0.051$ m (Table 1 and Case 3). Thus, $\Delta U_y = -0.08$ m, therefore, $\Delta U_f = -0.14$ m; −0.14 m and 0.131 m. Thus, based on the inflection point, these results have approximately equal values. This result in the fact that the maximum settlement obtained by the empirical formulas can be considered a reference for predicting ground settlement under undrained conditions.

4.1.2. The Effect of R/h on the Ground Deformation. Figure 9 shows the ground displacement with deformation points varying from −0.006 m to 0.046 m. (a) $U_y \max = -0.005$ m; $\Delta U_y = -0.004$ m and $\Delta U_f = 0.028$ m; (b) $U_y \max = -0.003$ m; $\Delta U_y = -0.037$ m and $\Delta U_f = 0.027$ m; (c)

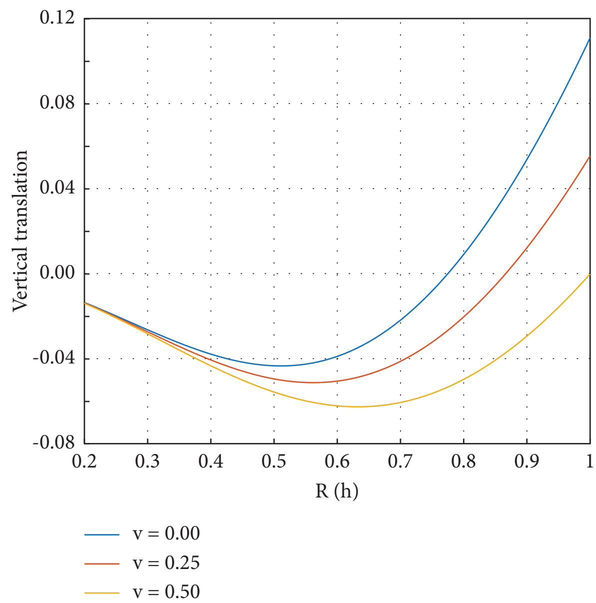

Figure 7: Vertical translation.

U_y max = −0.005 m; $\Delta U_y = -0.006$ m and $\Delta U_f = 0.039$ m; (d) U_x max = −0.007 m; $\Delta U_y = -0.008$ m, and $\Delta U_f = 0.046$ m, Thus, using equation (6), U_0 is obtained as −0.032 m, −0.064 m, −0.045 m, and −0.054 m respectively. The values of U_0 are between −0.03 m and −0.06 m. Furthermore, the settlement trough is estimated to be $R/h = 0.38$. This indicates that despite the load on the ground surface, the symmetrical distribution of the stresses induced by the ground traction can also cause ground loss and settlement around the cylindrical cavity.

4.2. Ground Displacement. Table 2 summarises the analytical data resulting from the selected cylindrical cavity. The modelling parameters are R/h, v, and u_ε.

4.2.1. Effect of V_L and v on the U_y max. The effect of ground loss can be an important factor in the maximum ground settlement around the cavity. Using data from the analytical formulas (equation (36)), the vertical displacement shown in Figure 10 depending on the values of v for $v = 0.00$, U_y max = −0.035 m, for $v = 0.25$, U_y max = −0.027 m, and for $v = 0.50$, U_y max = −0.018 m. Because the values of U_y max and V_L are close to the data obtained from the numerical results, we noted that the maximum ground settlement for different values of v is close to the empirical values. Therefore, v also influences the ground loss and considers the settlement trough. The result is that the variations of v can also contribute to the ground deformation around a cylindrical cavity.

4.2.2. The Effect of U_x/U_y and i. The vertical translation of the ground is established based on u_ε and R/h. The observed displacement is plotted as a function of u_ε. The displacement Equations (29), (30), (32), and (33) are used for digitising the deformations shown in Figure 11. Because the load applied on the ground surface is not evaluable, the values of U_x and U_y show a variation of the stresses related to the load on the ground surface and with R/h. Interpreting Figures 11(a)–11(d), we notice that for (a) $U_x/U_y = -0.053$ m; (b) $U_x/U_y = -0.052$ m; (c) $U_x/U_y = -0.055$ m; and (d) $U_x/U_y = -0.054$ m. The values of u_ε are established based on V_L, so the intercession between U_x/U_y is considered the maximum ground settlement trough. Furthermore, for the inflection points (a), (b), (c), and (d), $i = -0.05$ m; this value is approximately equal to the value obtained by the empirical formulas ($i = \pm 0.061$ m).

4.2.3. Variation of the U_s max. Figure 12 shows the maximum vertical settlement resulting from equation (32). The numerical data used are given in Table 2. It should be noted that the ground settlement varies with the inflection point i. The values obtain the following maximum settlement: Table 2 and case 1: U_s max = −1.175 m and −1.32 m; Table 2 and case 2: U_s max = −0.875 m; and Table 2 and case 3: U_s max = −1.625 m, with $i = 0.061$ m. These results for the maximum ground settlement are approximately similar to the data.

5. Discussion

Figure 13 shows the superposition of the ground displacements under the variable u_ε. It can be seen that the settlement troughs all converge to the values $R/h = 0.0375$ and U_y max = −0.005 m. Because all curves converge to the same intercession point of coordinates (0.75; 0), it indicates that the pressure in the cavity centre is lower than the surface pressure; hence, the settlement effect on the ground surface.

The ground surface settles when the surface load exceeds the cavity axis pressure. Figure 14 shows the relationship between the empirical and analytical solutions. The codes

Table 1: Cases of tunneling and related maximum ground settlement (it should be noted that the model tests in Table 1, cases 2 and 3, are test data and can be performed under drained and undrained conditions).

No	PN[1]	EM[2]	R/h	U_x max[3] (m)	V_L (%)	u_ε (m)	Reference
1	WB crossrail tunnel beneath hyde park	EPB	0.12	1.12; 1.58; 1.86; 1.95; 2.22; 4.45; 10.31; 15.03	0.9; 1.3; 1.54; 1.61; 1.83; 3.67; 8.5; 12.4	0.04; 0.06; 0.07; 0.07; 0.08; 0.16; 0.38; 0.56	Ieronymaki et al. [55, 56]
2	Model test	EPB	0.31	1.24; 4.79; 5.15; 17.05	1.03; 3.95; 4.25; 14.06	0.40; 1.57; 1.69; 5.60	Hu et al. [57]
3	Model test	—	—	1.60; 1.90; 2.55; 10.91; 17.05	1.32; 1.32; 1.56; 2.10; 9; 14.06	0.21; 0.21; 0.24; 0.34; 1.43; 2.24	Wang et al. [58]

[1]PN: project name; [2]EM: excavation method. Noted: [3]U_x max is negative.

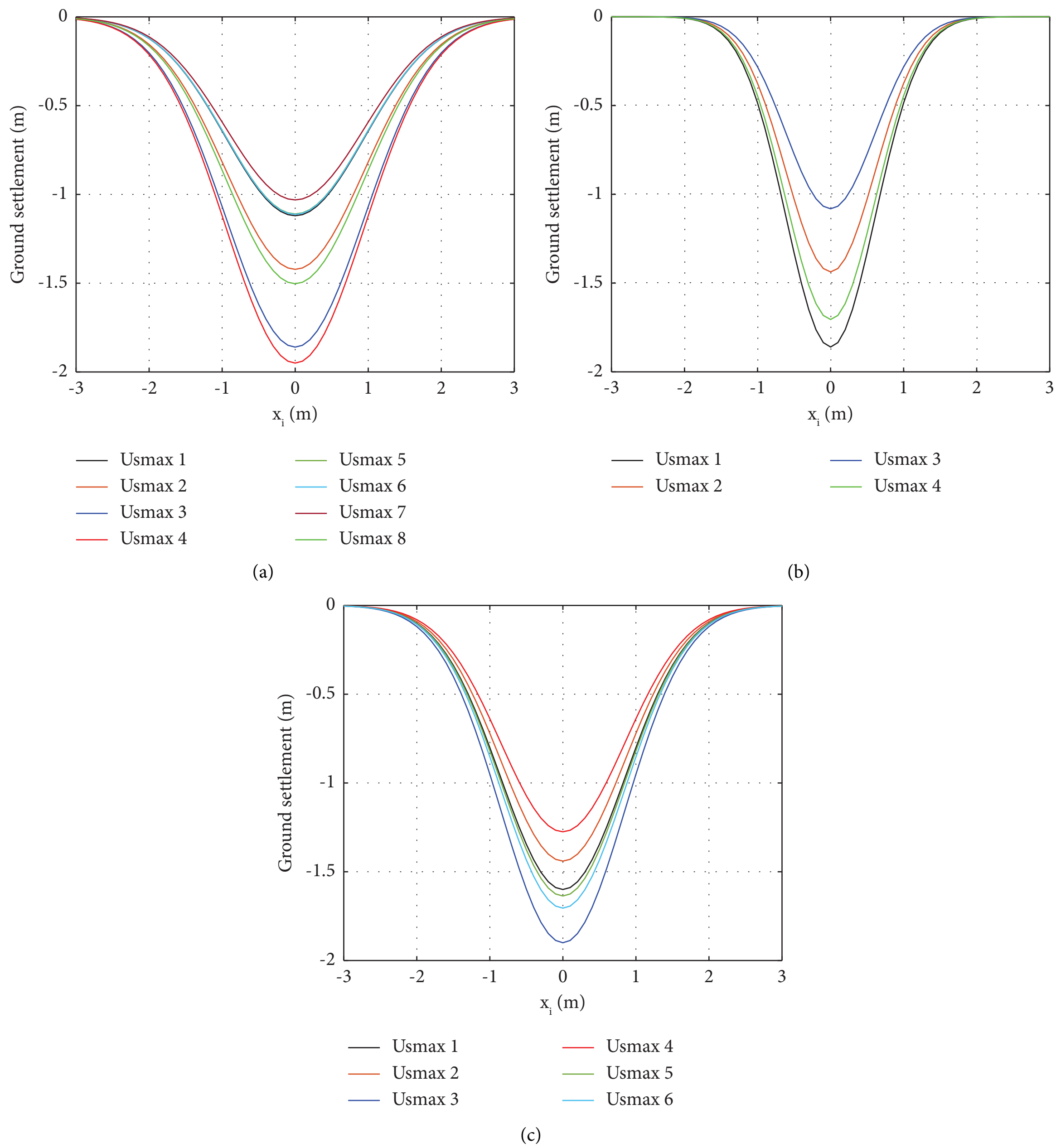

Figure 8: Maximum settlement predicted by the empirical method. (a) U_x max (Table 1 and case 1). (b) U_x max (Table 1 and case 2). (c) U_x max (Table 1 and case 3).

resulting from equation (27) are the input parameters for the numerical simulation. The interpretation of Figure 14 shows U_s max $= -1.3$ m (analytical result) and U_s max $= -1.4$ m (empirical result). These values are approximately equal to the results obtained in Sections 4.1.1 and 4.2 (iii). Since the empirical results are mainly based on the Gaussian distribution curve, this study has shown that the prediction of the ground settlement can also use the linear elastic soil problem to determine the maximum ground settlement.

Figure 15 shows the superposition of the maximum surface displacement depending on the effect of ν and V_L. The data obtained varies for values of $\nu = 0.00$, $\nu = 0.25$, and $\nu = 0.50$. It is observed that the settlement troughs all converge to $R/h = 1.5$. The vertical displacement is negative because the figure is represented by the equation $y - h = 0$. These data result from the synthesis of Tables 1 and 2.

Table 3 summarises the maximum vertical displacement as a function of ν and V_L. The values obtained are based on the formula for maximum settlement under undrained conditions. U_y max and U_0 are approximately similar to the previously obtained data. Although the empirical method usually determines the maximum settlement, this case study shows that, by using the harmonic conjugation with varying values of ν, the analytical approach can also give settlements symmetrical to the cross-section. Since the ground displacement is not only closely related to the ground stresses,

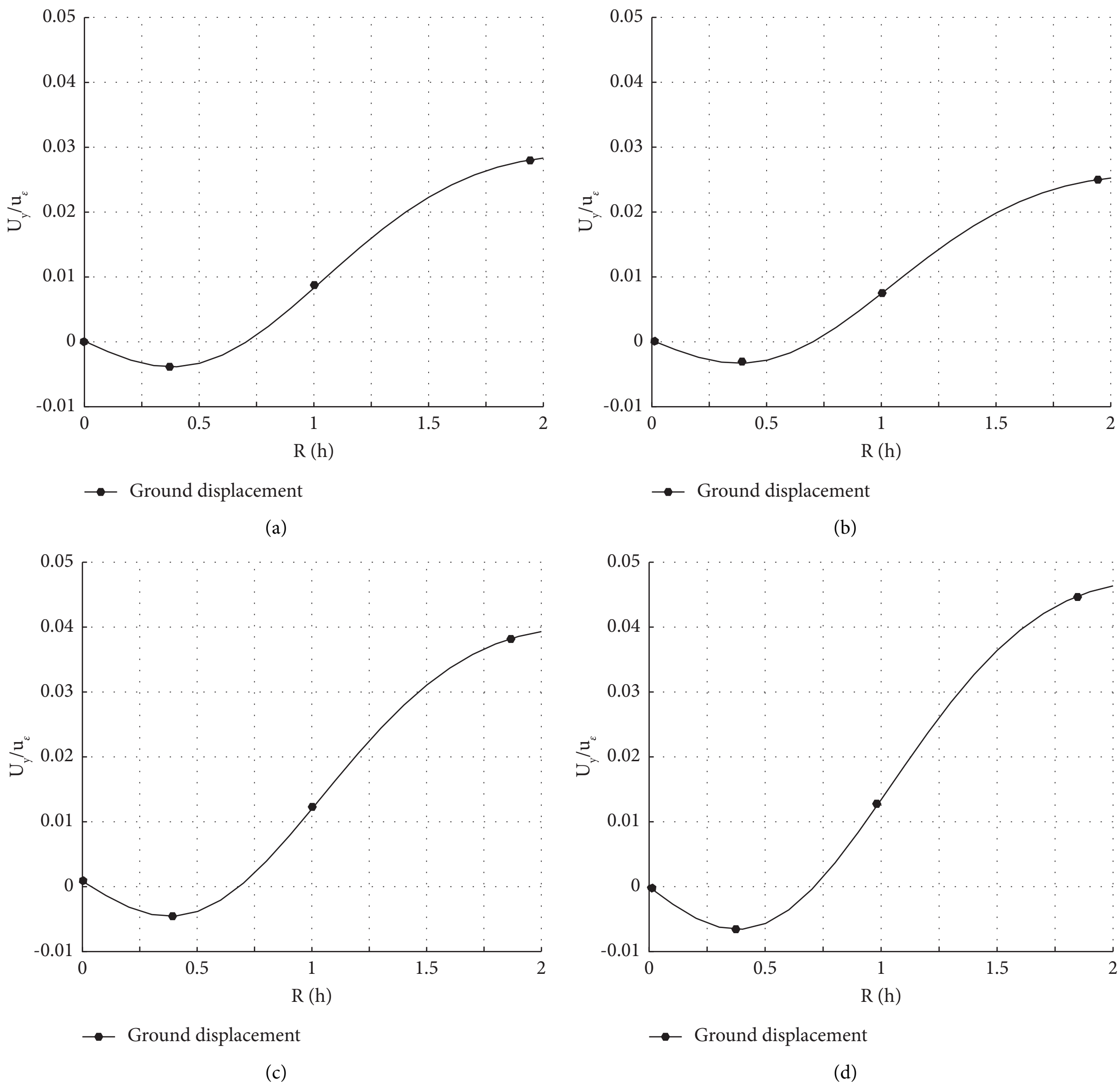

Figure 9: Ground displacement with variable u_ε. (a) $u_\varepsilon = 0.040$ m. (b) $u_\varepsilon = 0.041$ m. (c) $u_\varepsilon = 0.058$ m. (d) $u_\varepsilon = 0.068$ m.

Table 2: Some case studies.

No.	[1]PN	[2]EM	R/h	v	V_L (%)	u_ε (m)	Reference
1	Extension of madrid metro	EPB, slurry shield	0.29	0.50	0.25 7.2	−0.009; −0.26	Pinto et al. [52]
2	Sewer, cairo	(i) APS (ii) Slurry TBMs	0.19	0	1.2	−0.07	El-Nahhas et al. [59]
3	Lanzhou subway line 1	EPB, slurry shield	0.5; 0.34	0.25	35	−0.65	He et al. [60]

[1]PN: project name; [2]EM: excavation method.

the displacement can also be related to the variation of the intercession point. Thus, Figure 16 shows the superposition of the vertical translation established by (31), with the intercession point $x/h = 1$; U_x/u_ε and $U_y/u_\varepsilon = -0.0686$. U_x max = 0.1 m, U_x min = 0.06 m, and U_y max = −0.10 m and $x/h = 0$; these values are approximately equal to the empirical results. This specifies that the correlation between the empirical and analytical methods can best predict the ground deformation. Since the ground displacement is not only closely related to the ground stresses, the displacement can also be related to the variation of the intercession point. Thus, Figure 16 shows the superposition of the vertical translation established by (31), with the intercession point $x/h = 1$; U_x/u_ε and $U_y/u_\varepsilon = -0.0686$. U_x max = 0.1 m,

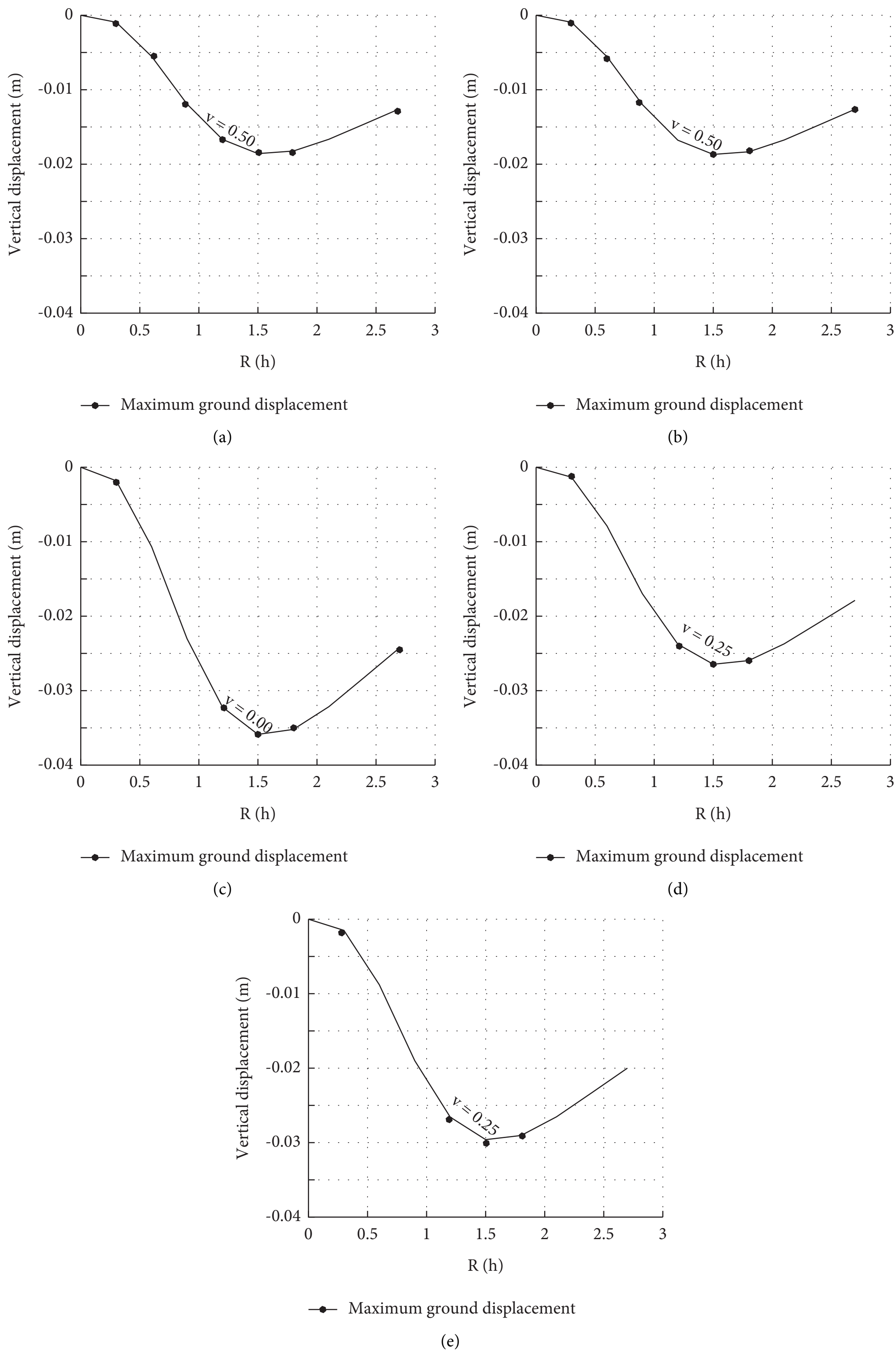

Figure 10: Maximum surface displacement due to the vertical displacement. (a) $V_L = -0.002\%$. (b) $V_L = -0.058\%$. (c) $V_L = -0.002\%$. (d) $V_L = -0.071\%$. (e) $V_L = -0.079\%$.

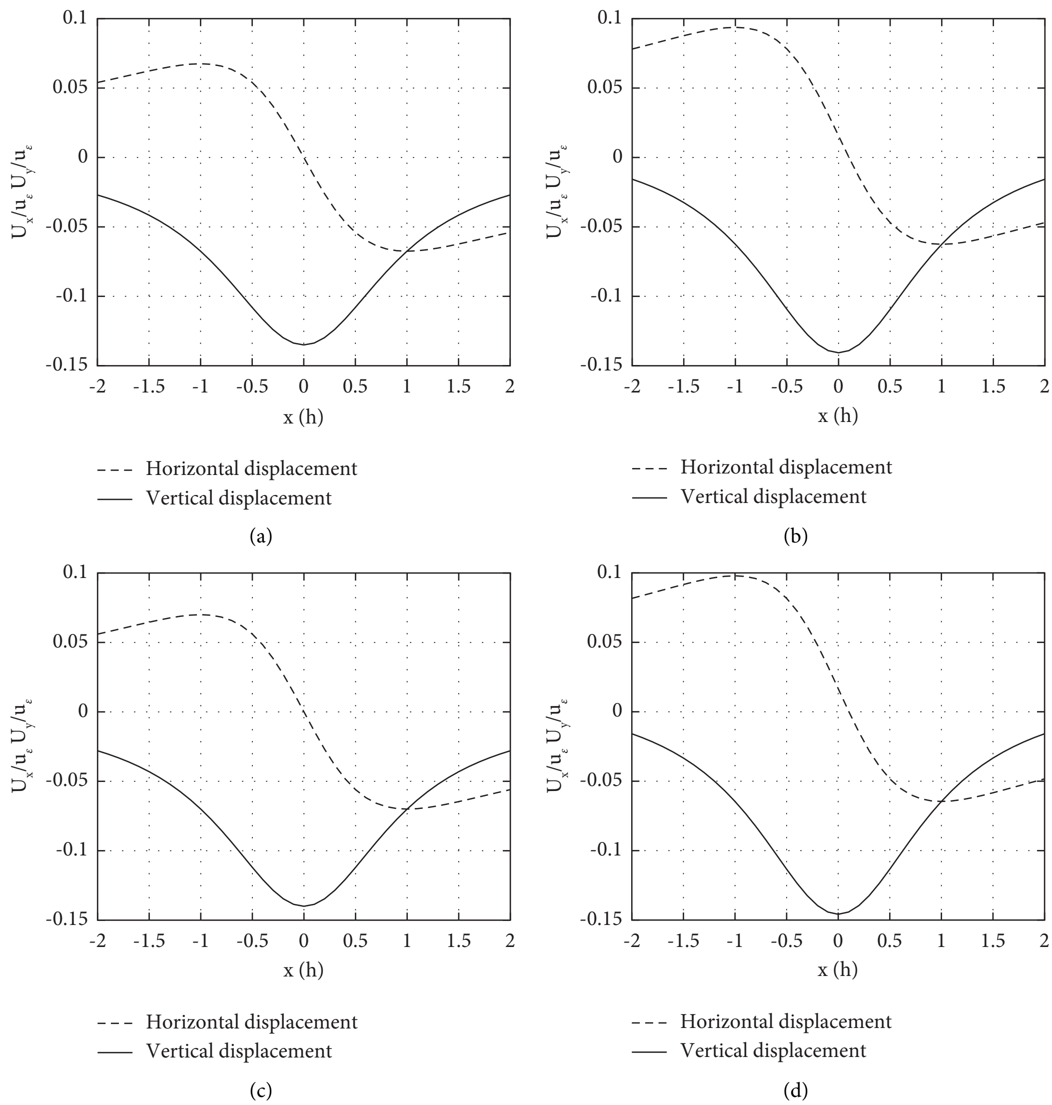

FIGURE 11: Vertical translation induced by u_ε. (a) $u_\varepsilon = 0.009$ m. (b) $u_\varepsilon = 0.25$ m. (c) $u_\varepsilon = 0.07$ m. (d) $u_\varepsilon = 0.56$ m.

U_x min = 0.06 m, and U_y max = −0.10 m and $x/h = 0$; these values are approximately equal to the empirical results. This specifies that the correlation between the empirical and analytical methods can best predict the ground deformation.

Figure 17 shows the relationship between the vertical translation (analytical formulas) and the experimental data. The settlement trough is $R/h = 0.4$. The settlement interval is between −0.06 m and −0.04 m. The intercession points are represented by the coordinates $\Delta U_y = 0.2$ and $\Delta U_y = -0.04$ m. These values are approximately equal to the initial displacement U_0 obtained in Section 4.1.1. Furthermore, according to the data on the effect of R/h resulting from the empirical analysis, these values are also related to the values of ΔU_y and ΔU_f presented in Section 4.1.2. Thus, the relationship between the empirical and analytical solutions can be a predictive tool for ground settlement around a cylindrical cavity under undrained conditions.

Figure 18 shows the relationship between the empirical and analytical solutions resulting from equations (26) and (36). The numerical data are ν, ΔU_y, and u_ε. The approach is based on the conformal vertical translation at the wall of the cylindrical cavity to obtain a displacement on both poles of the centre line. Using equations (27) and (36), the displacement given by the relationship between empirical and analytical formulas can be expressed as follows:

$$U_y \max = \pm 1.57 u_\varepsilon \left(\frac{R}{h}\right)\left\{\left\{(1-4(2-\nu))^2-5\right\}\left(x_i^2-0.03\right).\exp\left\{-\frac{x_i^2}{0.061}\right\}\left(\frac{R}{h}\right)+0.08\left\{-4(1-\nu)\left(\frac{R}{h}\right)^2+1\right\}\right\}. \quad (38)$$

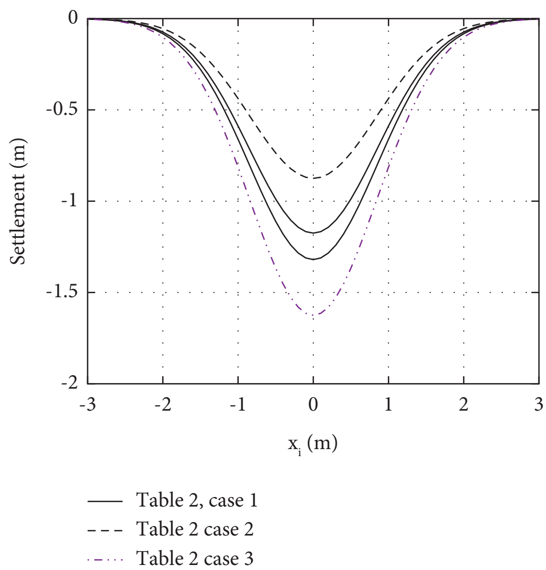

FIGURE 12: Ground settlement.

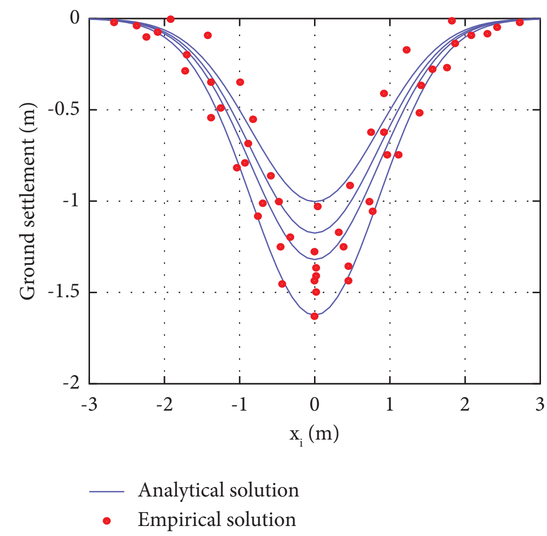

FIGURE 14: Relation between empirical solution and analytical solution.

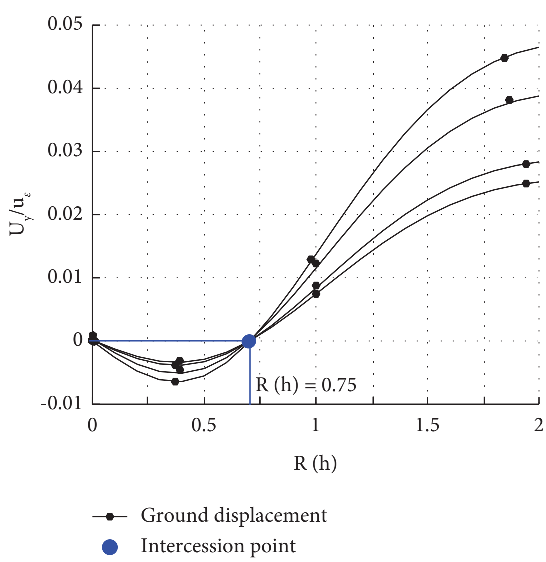

FIGURE 13: Superposition of ground displacement curves.

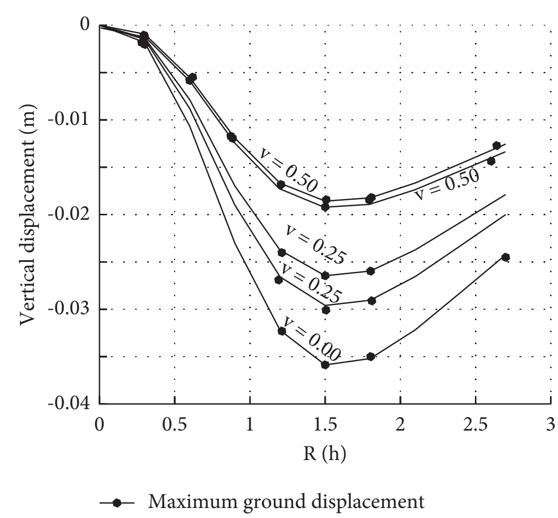

FIGURE 15: Superposition of maximum vertical displacement as a function of v and V_L.

Hence, the result presented in Figure 19 mathematizes the relationship between the two proposed approaches. The vertical translation could then be defined as the vertical displacement at the centreline of the cavity. Moreover, the settlement trough of both solutions is given by the value ΔU_y. Thus, taking into account the variation of the Poisson ratio, the empirical and analytical solutions present approximately equal results.

TABLE 3: Synthesis of maximum displacement and conformal convergence.

N°	v	U_y max (m)	U_0 (m)
1	0.00	−0.036	−0.06
2	0.25	−0.03 and −0.026	−0.06
3	0.50	−0.019	−0.051

6. Applying the Method in Practical Engineering

The undrained condition is a complex model to apply in practical engineering. Hence, this study adopted the undrained conditions to implement the compression mechanism of a stress model to evaluate ground settlement. In practice, adjacent high-rise buildings can produce a surcharge effect on a deep excavation (Guo et al. [61]). The planned cavity will be constructed using a tunneling machine, which requires reserving favourable conditions for the current excavation project (Guo et al. [62]). At each stage of excavation, the simulation of tunnel excavation consists of the following three substeps: removal of soil elements along a drive length, attachment of the created shell elements that

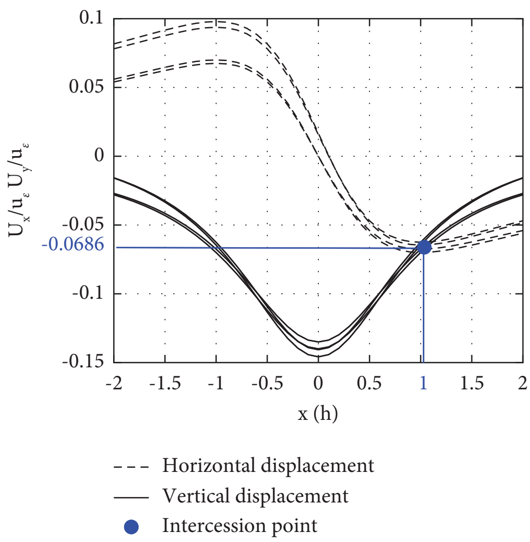

Figure 16: Superposition of the vertical translation induced by u_ε.

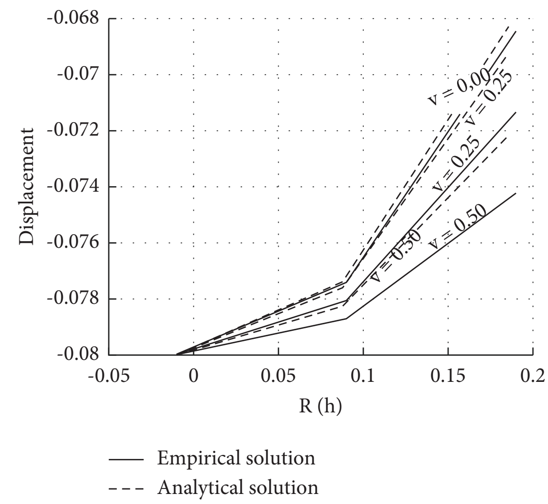

Figure 19: Relationship between ground settlement and maximum displacement.

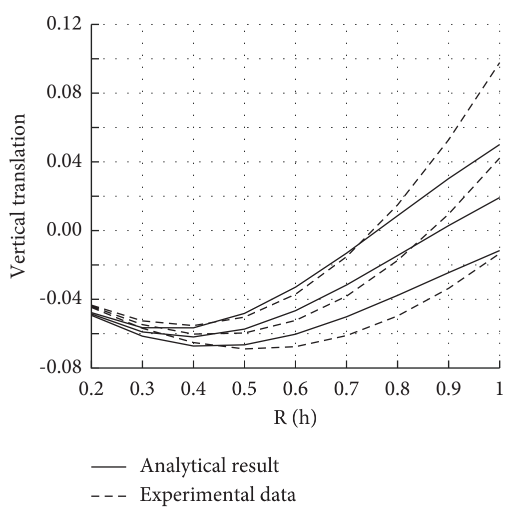

Figure 17: Relationship between the analytical result and the experimental data.

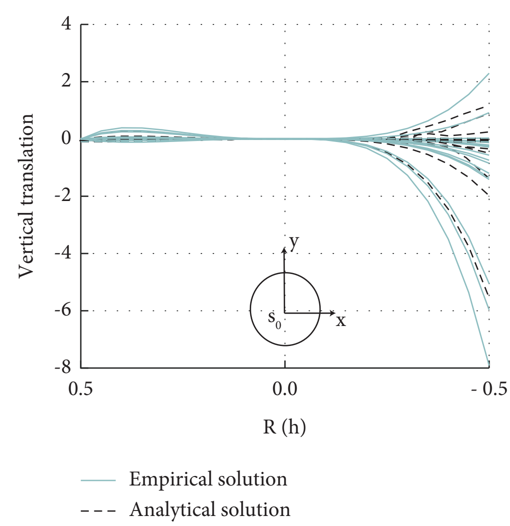

Figure 20: Practical results given by the relationship between the empirical and the analytical solution.

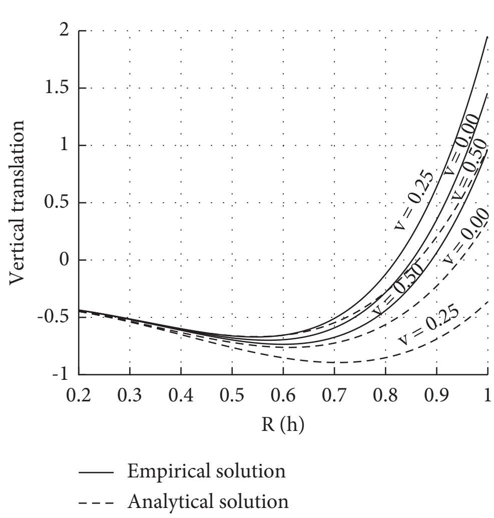

Figure 18: Relationship between the empirical method and the analytical method.

simulate the lining segments, and application of normal compressive pressure to the cavity face (Guo et al. [63]). Because of these restrictions, the excavation support system becomes complex, and the excavation results will inevitably differ from those of conventional excavations. It solves the problem of expanding the cylindrical cavity using parameters based on the uniaxial stress analysis. It should also help engineers to predict the weight of the load on the ground surface before excavation, even though it is variable.

A practical geotechnical problem is analysed in this study using the present solution. A deformation of the cavity radius usually describes the ground settlement problem around a cylindrical cavity. As the empirical prediction according to the Gaussian distribution curve has yet to be deeply adopted as a complete prediction tool, the stress evaluation of the upper layer is analysed to evaluate, with a high percentage, the ground settlement around a cylindrical cavity. In the current engineering, this method minimises the disturbances related to ground deformation and provides additional value to the reinforcement of the foundations around the cavity.

Figure 20 shows the superposition between the empirical and analytical results. Numerically, the results obtained by the empirical and analytical prediction show satisfactory results. For $-0.5 < R/h < 0.5$, the vertical translation induced by the curve moves horizontally along the centre line of the cylindrical cavity. It should be noted that, at $R/h = 0$, the curves all converge towards the central axis. This can be explained by the fact that internal pressure is almost non-existent. When the curves cross the central axis ($0 < R/h < 0.5$), the curves all diverge towards $R/h = 0.5$. Thus, in the practical domain, when the load on the ground surface is mobile, the compressive stresses can be redistributed towards the central axis of the cavity. The curves also show close values, indicating that the relationship between the analytical and empirical solutions can be best suited to predicting the ground settlement around a cavity. These data will support "piles" to model the expansion when the cylindrical cavity is shallow. Furthermore, the values obtained to allow the reduction of the stress rate concerning the ground weight and the reconstruction of the shear that can cause the "elongation" and therefore, the rupture of the cylindrical cavity cross-section.

7. Conclusions

This study proposes an approximate solution under undrained conditions, based on the relationship between the empirical and analytical methods for predicting ground settlement around a cylindrical cavity. A settlement technique is proposed based on the initial ground radial displacement influenced by conformal convergence and vertical translation. The method considers the excavation speed as the cause of settlement during the unloading process. Thus, a boundary condition study is conducted to estimate the origin of the cavity expansion by proposing a ground loss mechanism around the cylindrical cavity; then, a maximum displacement is induced by the vertical translation when the ground surface is subjected to a static load.

(1) An empirical prediction is first proposed by evaluating the settlement origin related to the variation of and the R/h ratio. The maximum settlement is determined by considering the cavity radius, the depth h and the ground surface h_0. Furthermore, the radial displacement is obtained using ground compression and decreasing the ground's internal pressure.

(2) Then, an analytical method is proposed by calculating the defined stresses based on the linear elasticity problem of the ground. An evaluation of the ground deformation is presented by determining at the boundary condition the hydrostatic pressure as the origin of the ground displacement. Using the Airy stress, shear stress, and compression force at the boundary condition, the ground final displacement state is determined with values of ν (0.00, 0.25, and 0.50) variables. These obtained displacements are used for digitising the contour lines and the vertical translation to evaluate the ground behaviour at the cavity wall and the maximum surface displacement, respectively.

(3) These results are converted into code to numerically evaluate the ground settlement around the cylindrical cavity using the MATLAB software. Some examples of cylindrical cavities are proposed to justify the mathematical equations. An evaluation is first established on the empirical solutions utilising the input parameters, V_L, u_ε, and U_s max. Subsequently, the analytical data were also proposed based on R/h, u_ε, and ν. The relationship between the two methods allowed the determination of the ground settlement and the maximum surface displacement induced by the cavity unloading process.

(4) A discussion based on the relationship between the mathematical formulas and the experimental data is proposed, and the results gave approximately similar values. Specifically, the relationship between the empirical and analytical solutions will be a better means to predict the ground settlement around a cylindrical cavity, thus, the load on the ground surface. In practice, the results could help engineers evaluate the stresses for reinforcing "support piles" and the "buoyancy effect" even though the ground surface load is variable.

Data Availability

All data, models, and code generated or used during the study are available from the corresponding author upon reasonable request.

Conflicts of Interest

The authors declare that they have no conflicts of interest.

Acknowledgments

This research was funded by the Beijing Natural Science Foundation, grant number "8222020." The authors would like to express their appreciation and thanks to Jia Le Zhao, Yong-Gwang Jong, and Njoke L. Mbanda for their suggestions for improving this work.

References

[1] H. W. Huang and D. Zhang, "Resilience analysis of shield tunnel lining under extreme surcharge: characterization and field application," *Tunnelling and Underground Space Technology*, vol. 51, pp. 301–312, 2016.

[2] Y. F. Yan, Q. Huang, Y. Xie et al., "Failure analysis and deformation mechanism of segmented utility tunnels crossing ground fissure zones with different intersection angles,"

Engineering Failure Analysis, vol. 139, Article ID 106456, 2022.
[3] A. Klar and A. M. Marshall, "Linear elastic tunnel pipeline interaction: the existence and consequence of volume loss equality," *Géotechnique*, vol. 65, no. 9, pp. 788–792, 2015.
[4] A. Klar, I. Elkayam, and A. Marshall, "Design oriented linear equivalent approach for evaluating the effect of tunneling on pipelines," *Journal of Geotechnical and Geoenvironmental Engineering*, vol. 142, no. 1, Article ID 04015062, 2016.
[5] V. Avgerinos, D. M. Potts, and J. R. Standing, "Numerical investigation of the effects of tunnelling on existing tunnels," *Géotechnique*, vol. 67, no. 9, pp. 808–822, 2017.
[6] K. Haji, A. Marshall, and W. Tizani, "A cantilever approach to estimate bending stiffness of buildings affected by tunnelling," *Tunnelling and Underground Space Technology*, vol. 71, pp. 7147–7161, 2018.
[7] D. Lu, F. Kong, X. Du, C. Shen, Q. Gong, and P. Li, "A unified displacement function to analytically predict ground deformation of shallow tunnel," *Tunnelling and Underground Space Technology*, vol. 88, pp. 129–143, 2019.
[8] Z. Zhang, M. Huang, C. Zhang, K. Jiang, Z. Wang, and X. Xi, "Complex variable solution for twin tunneling-induced ground movements considering nonuniform convergence pattern," *International Journal of Geomechanics*, vol. 20, no. 6, Article ID 0402006, 2020.
[9] H. –N. Wu, S. –L. Shen, and J. Yang, "Identification of tunnel settlement caused by land subsidence in soft deposit of shanghai," *Journal of Performance of Constructed Facilities*, vol. 31, no. 6, Article ID 04017092, 2017.
[10] R. B. Peck, "Deep excavation and tunneling in soft ground," State of the Art Report, pp. 225–290, ISSMGE, Colombo, Sri Lanka, 1969.
[11] B. Schmidt, "Settlement and ground movement associated with tunneling in soil," Ph. D. Thesis, University of Illinois, Urbana, Illinois, USA, 1969.
[12] T. B. Celestino, R. A. M. P. Gomes, and A. A. Bortolucci, "Errors in-ground distortions due to settlement trough adjustment," *Tunnelling and Underground Space Technology*, vol. 15, no. 1, pp. 97–100, 2000.
[13] P.-Q. Mo, A. M. Marshall, and H. –S. Yu, "Elastic-plastic solutions for expanding cavities embedded in two different cohesive-frictional materials," *International Journal for Numerical and Analytical Methods in Geomechanics*, vol. 38, no. 9, pp. 961–977, 2014.
[14] G. Gioda and G. Swoboda, "Developments and applications of the numerical analysis of tunnels in continuous media," *International Journal for Numerical and Analytical Methods in Geomechanics*, vol. 23, no. 13, pp. 1393–1405, 1999.
[15] C. L. Gao, Z. Q. Zhou, W. M. Yang, C. J. Lin, L. P. Li, and J. Wang, "Model test and numerical simulation research of water leakage in operating tunnels passing through intersecting faults," *Tunnelling and Underground Space Technology*, vol. 94, Article ID 103134, 2019.
[16] Z. C. Wang, G. D. Li, A. X. Wang, and K. Pan, "Numerical simulation study of stratum subsidence induced by sand leakage in tunnel lining based on particle flow software," *Geotechnical and Geological Engineering*, vol. 38, no. 4, pp. 3955–3965, 2020.
[17] H. N. Wu, S. L. Shen, R. P. Chen, and A. N. Zhou, "Three-dimensional numerical modelling on localised leakage in segmental lining of shield tunnels," *Computers and Geotechnics*, vol. 122, no. 3, Article ID 103549, 2020.
[18] Z. G. Zhang, M. D. Mao, Y. T. Pan et al., "Experimental study for joint leakage process of tunnel lining and particle flow numerical simulation," *Engineering Failure Analysis*, vol. 138, Article ID 106348, 2022.
[19] S. C. Möller and P. A. Vermeer, "On numerical simulation of tunnel installation," *Tunnelling and Underground Space Technology*, vol. 23, no. 4, pp. 461–475, 2008.
[20] A. Amorosi, D. Boldini, G. De Felice, M. Malena, and M. Sebastianelli, "Tunnelling-induced deformation and damage on historical masonry structures," *Géotechnique*, vol. 64, no. 2, pp. 118–130, 2014.
[21] R. Hasanpour, "Advance numerical simulation of tunneling by using a double shield TBM," *Computers and Geotechnics*, vol. 57, pp. 5737–5752, 2014.
[22] G. Zheng, P. Lu, and Y. Diao, "Advance speed-based parametric study of greenfield deformation induced by EPBM tunneling in soft ground," *Computers and Geotechnics*, vol. 65, pp. 220–232, 2015.
[23] G. Zheng, T. Zhang, and Y. Diao, "Mechanism and countermeasures of preceding tunnel distortion induced by succeeding EPBS tunnelling in close proximity," *Computers and Geotechnics*, vol. 66, pp. 53–65, 2015.
[24] Z. Zhang, M. Huang, and M. Zhang, "Theoretical prediction of ground movements induced by tunnelling in multi-layered soils," *Tunnelling and Underground Space Technology*, vol. 26, no. 2, pp. 345–355, 2011.
[25] Z. Zhang, M. Huang, X. Xi, and X. Yang, "Complex variable solutions for soil and liner deformation due to tunneling in clays," *International Journal of Geomechanics*, vol. 18, no. 7, Article ID 04018074, 2018.
[26] X. L. Lü, Y. C. Zhou, M. Huang, and S. Zeng, "Experimental study of the face stability of shield tunnel in sands under seepage condition," *Tunnelling and Underground Space Technology*, vol. 74, pp. 195–205, 2018.
[27] C. Sagaseta, "Analysis of undrained soil deformation due to ground loss," *Géotechnique*, vol. 37, no. 3, pp. 301–320, 1987.
[28] A. Verruijt and J. R. Booker, "Surface settlements due to deformation of a tunnel in an elastic half plane," *Géotechnique*, vol. 46, no. 4, pp. 753–756, 1996.
[29] A. Verruijt, "A complex variable solution for a deforming circular tunnel in an elastic half-plane," *International Journal for Numerical and Analytical Methods in Geomechanics*, vol. 21, no. 2, pp. 77–89, 1997.
[30] K.-H. Park, "Analytical solution for tunnelling-induced ground movement in clays," *Tunnelling and Underground Space Technology*, vol. 20, no. 3, pp. 249–261, 2005.
[31] L.-Z. Wang, L.-L. Li, and X.-J. Lv, "Complex variable solutions for tunneling-induced ground movement," *International Journal of Geomechanics*, vol. 9, pp. 63–72, 2009.
[32] F. Pinto and A. J. Whittle, "Ground movements due to shallow Tunnels in soft ground. I: analytical solutions," *Journal of Geotechnical and Geoenvironmental Engineering*, vol. 140, no. 4, Article ID 04013040, 2014.
[33] P. Mabe Fogang, Y. Liu, J. L. Zhao, and K. I. Azeuda Ndonfack, "Soil deformation around a cylindrical cavity under drained conditions: theoretical analysis," *Advances in Civil Engineering*, vol. 2022, pp. 1–15, 2022.
[34] A. Verruijt and J. R. Booker, "Complex variable analysis of Mindlin's tunnel problem," in *Proceedings of the Booker Memorial Symposium, Developments in Theoretical Geomechanics*, pp. 3–22, Balkema, Rotterdam, Netherlands, January 2000.
[35] A. Bobet, "Analytical solutions for shallow tunnels in saturated ground," *Journal of Engineering Mechanics*, vol. 127, pp. 1258–1266, 2001.

[36] H. S. Yu and R. K. Rowe, “Plasticity solutions for soil behaviour around contracting cavities and tunnels,” *International Journal for Numerical and Analytical Methods in Geomechanics*, vol. 23, pp. 1245–1279, 1999.
[37] R. J. Mair, “Tunnelling and geotechnics: new horizons,” *Géotechnique*, vol. 58, no. 9, pp. 695–736, 2008.
[38] J. Li, L. Li, D. Sun, and P. Rao, “Analysis of undrained cylindrical cavity expansion considering three-dimensional strength of soils,” *International Journal of Geomechanics*, vol. 16, no. 5, Article ID 04016017, 2016b.
[39] H. H. Chen, L. Li, J. P. Li, and H. Wang, “Stress transform method to undrained and drained expansion of a cylindrical cavity in anisotropic modified cam-clay soils,” *Computers and Geotechnics*, vol. 106, pp. 128–142, 2019.
[40] J. Zhang, L. Li, and D. Sun, “Similarity solution for undrained cylindrical cavity contraction in anisotropic modified Cam-clay model soils,” *Computers and Geotechnics*, vol. 120, Article ID 103405, 2020.
[41] S. L. Chen and Y. N. Abousleiman, “Exact undrained elasto–plastic solution for cylindrical cavity expansion in modified Cam Clay soil,” *Géotechnique*, vol. 62, no. 5, pp. 447–456, 2012.
[42] S. L. Chen, K. Liu, J. Castro, and N. Sivasithamparam, “Discussion on ‘Undrained cylindrical cavity expansion in anisotropic critical state soils,” *Géotechnique*, vol. 69, Article ID 1026e1028, 2019.
[43] C. Yang, H. Chen, and J. Li, “Drained cylindrical cavity expansion analysis in anisotropic soils considering 3D strength,” *Géotechnique Letters*, vol. 10, no. 2, pp. 346–352, 2020.
[44] A. Vrakas, “A rigorous semi-analytical solution for undrained cylindrical cavity expansion in critical state soils,” *International Journal for Numerical and Analytical Methods in Geomechanics*, vol. 40, no. 15, pp. 2137–2160, 2016.
[45] L. Hou, X. Weng, J. Hu, and R. Zhou, “Undrained semi-analytical solution for cylindrical cavity expansion in anisotropic soils under biaxial stress conditions,” *Journal of Rock Mechanics and Geotechnical Engineering*, pp. 1674–7755, 2022.
[46] Z. Zhai, Y. Zhang, S. Xiao, and T. Li, “Undrained elastoplastic solution for cylindrical cavity expansion in structured cam clay soil considering the destructuration effects,” *Applied Sciences*, vol. 12, no. 1, p. 440, 2022.
[47] P. –Z. Zhuang, H. Yang, H. –Y. Yue, R. Fuentes, and H. –S. Yu, “Plasticity solutions for ground deformation prediction of shallow tunnels in undrained clay,” *Tunnelling and Underground Space Technology*, vol. 120, Article ID 104277, 2022.
[48] C. M. Gerrard, “Tables of stresses, strains and displacements in two-layer elastic systems under various traffic loads,” *Australian Road Research Board Internal Report*, vol. 3, 1969.
[49] N. Sivasithamparam and J. Castro, “Undrained expansion of a cylindrical cavity in clays with fabric anisotropy: theoretical solution,” *Acta Geotech*, vol. 13, no. 3, pp. 729–746, 2017.
[50] H. G. Poulos, “The settlenent of under-reamed and step-taper piles,” *Civ. Fng.Trans. Inst.of Engrs.*, pp. 83–87, 1696.
[51] H. G. Poulos and E. H. Davis, *Elastic Solution for Soil and Rock*, The University of Sydney, Camperdown, Australia, 1974.
[52] F. Pinto, D. M. Zymnis, and A. J. Whittle, “Ground movements due to shallow tunnels in soft ground. II: analytical interpretation and prediction,” *Journal of Geotechnical and Geoenvironmental Engineering*, vol. 140, no. 4, Article ID 0401304, 2014.
[53] M. P. O’Reilly and B. M. New, “Settlements above tunnels in the United Kingdom-their magnitude and prediction,” *Tunnelling*, vol. 82, pp. 173–181, 1982.
[54] R. J. Mair, R. N. Taylor, and A. Bracegirdle, “Subsurface settlement profiles above tunnels in clays,” *Géotechnique*, vol. 43, no. 2, pp. 315–320, 1993.
[55] E. S. Ieronymaki, A. J. Whittle, and D. S. Sureda, “Interpretation of free-field ground movements caused by mechanized tunnel construction,” *Journal of Geotechnical and Geoenvironmental Engineering*, vol. 143, no. 4, Article ID 04016114, 2017.
[56] E. Ieronymaki, A. J. Whittle, and H. H. Einstein, “Comparative study of the effects of three tunneling methods on ground movements in stiff clay,” *Tunnelling and Underground Space Technology*, vol. 74, pp. 167–177, 2018.
[57] X. Y. Hu, Q. X. Yan, C. He, and X. Y. Yang, “Study on the disturbance and excavation face failure feature of granular mixtures stratum due to EPB shield tunneling,” *Chinese Journal of Mechanical Engineering*, vol. 35, pp. 1618–1627, 2016.
[58] F. Wang, L. Miao, X. M. Yang, Y. J. Du, and F. Y. Liang, “The volume of settlement trough change with depth caused by tunneling in sands,” *KSCE Journal of Civil Engineering*, vol. 20, no. 7, pp. 2719–2724, 2016.
[59] F. M. El-Nahhas, A. A. Ahmed, and K. A. Esmail, “Prediction of ground subsidence above tunnels in Cairo,” in *Proceedings of the 14th Int. Conf. Mech. Found. Eng*, vol. 3, pp. 1453–1456, Hamburg, Germany, September 1997.
[60] S. He, C. Li, D. Wang, and X. Liu, “Surface settlement induced by slurry shield tunnelling in sandy cobble strata—a case study,” *Indian Geotechnical Journal*, vol. 51, no. 6, pp. 1349–1363, 2021.
[61] P. Guo, X. Gong, and Y. Wang, “Displacement and force analyses of braced structure of deep excavation considering unsymmetrical surcharge effect,” *Computers and Geotechnics*, vol. 113, Article ID 103102, 2019.
[62] P. Guo, X. Gong, Y. Wang, H. Lin, and Y. Zhao, “Analysis of observed performance of a deep excavation straddled by shallowly buried pressurized pipelines and underneath traversed by planned tunnels,” *Tunnelling and Underground Space Technology*, vol. 132, Article ID 104946, 2023.
[63] P. Guo, X. Gong, Y. Wang, H. Lin, and Y. Zhao, “Minimum cover depth estimation for underwater shield tunnels,” *Tunnelling and Underground Space Technology*, vol. 115, Article ID 104027, 2021.